Journal of Engineering and Sustainable Development
http://jeasd.uomustansiriyah.edu.iq/index.php
https://doi.org/10.31272/jeasd.25.4.7

Vol. 25, No. 04, July 2021
ISSN 2520-0917

EFFECT OF ALUMINUM FOILS NUMBER AND ITS LENGTH IN IMPROVEMENT OF ELECTRIC FIELD DISTRIBUTION OF HIGH VOLTAGE CONDENSER

***Zahraa G. Mustafa[1]** **Kassim R. Hameed[1]**

1) Electrical Engineering Department, College of Engineering, Mustansiriyah University, Bagdad, Iraq

Received 29/12/2020 ***Accepted in revised form 22/2/2021*** ***Published 1/7/2021***

Abstract: High voltage condenser bushing is one of the important component that is widely used in the high voltage system. At high voltage levels more than 52kV the distribution of electric field in condenser bushing is irregular between the lead conductor and the grounded metallic flange. This paper studied the effects of changing in both: the number layers of aluminum foils and Oil impregnated Paper (OIP), increasing the length of aluminum foils layers, and also increasing the thickness of OIP layer on the distribution of electric potential and electric field in condenser bushing by using Finite Element Method (FEM) and built the bushing model in ANSYS software. The harmonic analysis was performed of the bushing model at maximum value of withstand voltage test at 50Hz, from the analysis results are obtained the maximum value of electric field on the inner and outer surface of the bushing, the obtained electric field values were good and acceptable compared to the permissible electrical stress values of the dielectric insulators. This work can also aid in the design of high voltage bushing stress control, a knowledge of the electrical field distribution in bushing geometry. Moreover the results of analysis are shown as contour plots, graphs plotted, and tables.

Keywords: *aluminum foils, condenser bushing, finite element method, oil impregnated paper.*

1. Introduction

Condenser Bushings are used in high voltage transformers to insulate the high voltage lead conductor from the earthed body of the transformer tank [1]-[3].

A high electric field intensity may cause punctures of inner insulating material or flashover along the external surface of bushings, a puncture occurrence depends on the radial stress of the insulating material, while flashover occurrence depends on the axial stress of the external surface of the bushing [2]. Publications on bushing theories can be found commonly in previous literature [2-6], most of the papers transact with a bushing having a finite number of aluminum foils.

Bushing faults case most power transformer failures, therefore the analysis of electric field distribution inside and outside the surface of high-voltage bushings is very important to improve the reliability of the power network [7].

Most bushing failures are attributed to moisture ingress, moisture inside a bushing decreases the dielectric strength and life of the insulation, thus increasing the chance of unexpected failure, and failure of bushing doesn't only destroy the transformer but also leads to major damage to the power transmission network [8].

The material used in the bushing must have a high dielectric strength and mechanical strength sufficient to support the lead conductor, a most

**Corresponding Author*: zahraaghalib17@gmail.com

power transformer failures are caused by bushing faults, the analysis of electric field distribution inside and on the output surface of high-voltage bushings is very important to improve the reliability of the power network [9].

Modern high-voltage bushings with oil-paper insulation are condenser-type for system voltages greater than 52 kV. The condenser bushing contains central conductor and aluminum ground flange separate them the layers of insulation paper and thin aluminum foil, where these are wrapped on the conductor tightly, then immerse
oil insulation. Aluminum foil layers within oil insulation paper take the shape of coaxial cylinders and constitute a series of cylindrical condensers, design in such a way that the electrical stress in both radial and axial directions does not exceed the critical values. The capacitance between any adjacent pair of aluminum foils is known as partial capacitance, the bushing insulation contains a large number of partial condenser in series. Optimum number of foils and the dimensions of each foil result in appropriate dielectric stresses and the most economical design of the insulation system [5, 10].

The Finite Element Method (FEM) has proven to be very effective for electric field analysis systems in two-dimensional (2-D) axial-symmetric, and three-dimensional (3-D) with multiple dielectric media. FEM is a powerful tool and widely used in many engineering applications [4]. This paper, used the two dimensional axial- symmetrical model geometric of high voltage condenser bushing and built it in ANSYS software. The 2D analysis enables calculation of the electric field and its distribution in the entire system and allows maximum electrical field intensity in insulation to be calculated which it could not be analytically evaluated because of its complex geometrical shape [9].

2. Methodology

2.1. Bushing Configuration

The bushing used in this paper is a 72.5kV OIP condenser bushing, the main parts of this bushing shown in fig.1 [11].

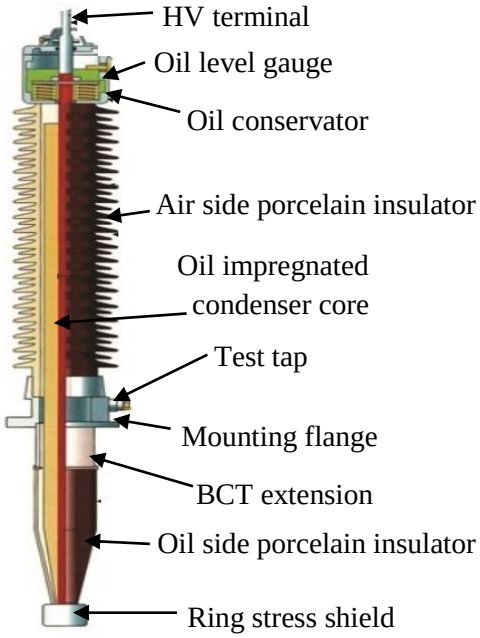

Figure.1 Main parts of OIP condenser bushing [11]

The internal and external dimensions of the bushing have been measured practically in Diyala Company Electrical Industries / Power Transformers Factory. Some main dimensions of this bushing structure are listed in Table.1

Table.1 main dimensions of 72.5kV OIP condenser bushing structure

Item	Parameters (mm)
Total length of bushing	1760
Diameter of lead conductor	45
Diameter of large sheds	250
Diameter of the small sheds	216
Length of upper porcelain (air side)	700
Length of lower porcelain (oil side)	255
Diameter of lower porcelain (oil side)	130
Length of stress shield	60
Diameter of stress shield	120

The condenser body is composed of 17 layer of OIP, the thickness of these layers alternates between 1.1 mm to 1.2 mm, and 16 layer of aluminum foils the thickness of each layer is 0.025mm, except the last layer which thick is 0.13mm.

The last layer of aluminum foils represents an internal ground electrode connected to the test tap, which is used for measurement and diagnosing purposes [1].

2.2. Electric Field Analysis Equations

The electric field analysis of any high voltage equipment is the important investigation for designing considerations, the efficient design of high voltage equipment requires calculation of the maximum value of electric stress that occurs in and around the electric equipment during the design stage in order to be reduced. The electric field distribution of an insulator depends on the geometry, material, and distribution of external contamination. In condenser bushing the condenser body has a major impact on the electric field distribution. [3].

OIP condenser bushing is the one of the high voltage equipment whose behavior can be described by field equations, the electric field in the inner and outer surface of the bushing are described by Maxwell's equations. Maxwell's equation will be employed to determine the potential and electric field, the relationship between the electric potential and electric Field is written as follows [6, 12]:

$$\mathrm{E} = -\nabla \mathrm{V} \quad (1)$$

From Maxwell's equation:

$$\nabla . E = \frac{\rho}{\varepsilon} \quad (2)$$

Where

ρ: Electric charge density.

ε: Permittivity of dielectric material ($\varepsilon = \varepsilon_o \varepsilon_r$).

ε_o: Air or space permittivity (8.854×10^{-12}F m^{-1}).

ε_r: Relative permittivity of dielectric material.

Poisson can be obtain by substituting equation (1) into (2) resulted it:

$$\nabla^2 V = -\frac{\rho}{\varepsilon} \quad (3)$$

For zero charge density equation (3) reduces to Laplace's equation:

$$\nabla^2 V = 0 \quad (4)$$

2.2. Building the Finite Element Model

To build the OIP condenser bushing model in the ANSYS window, there are two ways: either using the Graphical User Interface (GUI) mode or ANSYS Programming Design Language (APDL). In this paper, the OIP condenser model is used by using the APDL mode according to the steps followed in ANSYS package. For building the finite element model of condenser bushing generally, there are six steps for the finite element analysis:

1. Build the geometry of bushing.
2. Assign the electric properties of each material in this model.
3. Mesh for all the region of the model
4. Assign load and boundary conditions.
5. Solve the field with proper solver.
6. Post processing.

Build the geometry of bushing requires practical measuring the inner and outer dimensions of the bushing accurately, the dimensions of this bushing were taken in Diyala Company for electrical industries. Building the model started first from Key -points, secondly connecting these Key points by lines from these lines areas will be created, this the procedure is followed to build any model in ANSYS software. Since the OIP condenser bushing is a symmetric geometry, it can be used the symmetric axis model as shown in Fig.2.The bushing model is made of seven different materials [1]:

1. Air: the surrounding medium of the upper part of bushing.
2. Porcelain: the bushing housing consisting of an upper (air side) and a lower (submerged in oil).
3. Aluminum: flange, oil conservator, and stress shield.
4. Aluminum foils: grading foils between insulation paper layers.
5. Copper: lead conductor and HV outer terminal.
6. Insulating paper (OIP): paper layers impregnated with oil.
7. Oil: insulation for filling inside the bushing and transformer tank**.**

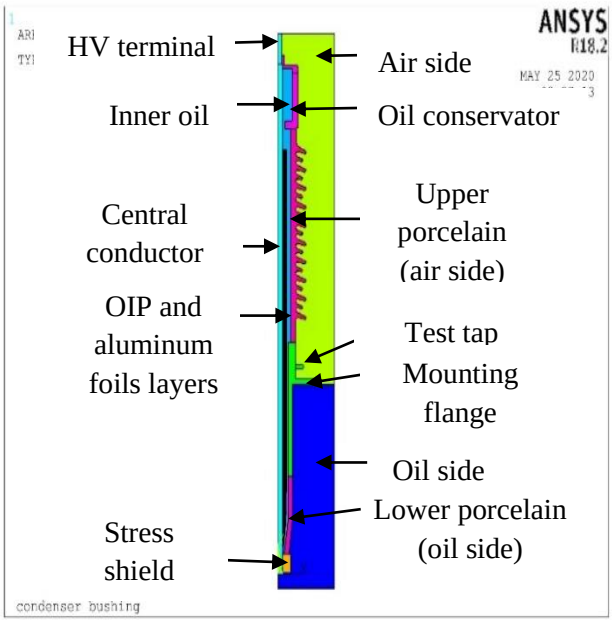

Figure 2. (2-D) axisymmetric model of OIP condenser bushing

The electric properties (permittivity and electrical resistivity) are applied in each area of the model, Table.2 shows the properties for each materials in the bushing model [13].

The different colors in fig.2 indicate the difference in parts and materials of the bushing.

Table.2 Parameters for each materials in the model

Materials	Relative dielectric constant	Volume resistivity (Ωcm)
Insulating oil (mineral oil)	2.2-2.4	7.6×10^{15}
Kraft paper (insulation paper)	3.5-4.2	2.4×10^{15}
porcelain	6	10^{14}
Air	1	1×10^{15}
Conductor	1	1.72×10^{-8}
Aluminum	1	2.82×10^{-8}
Aluminum foils	10000	2.82×10^{-8}

The electric potential and electric field have been calculated and their distribution in this bushing by using harmonic analysis for the 2D model, the element type is plane230 (8 nodes, 2-D), also the model consists of (864621) elements and (1358725) nodes. Fig.3 shows the element mesh in the bushing model.

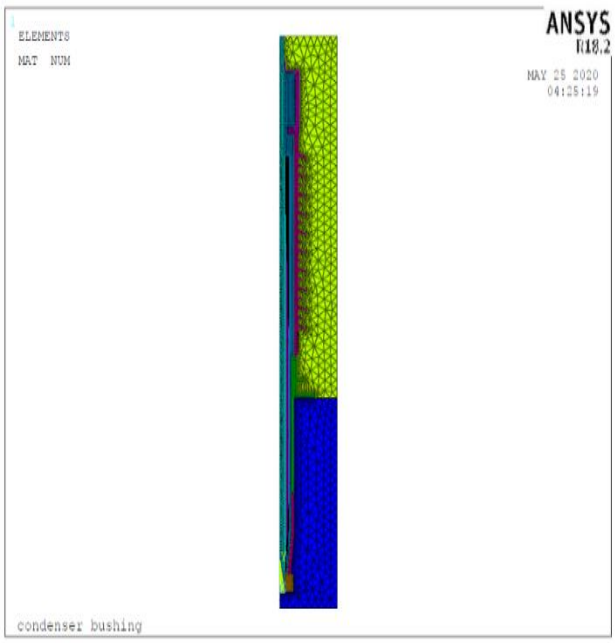

Figure 3. (2-D) Finite element mesh of OIP condenser bushing

2.2.1. *Complete Model*

The complete bushing model was shown in fig.2, where the area of mineral oil inside the

bushing was obtained by using the overlap operation for all areas. After merging the coincident nodes and compressing the node numbers, the FE model would be ready for the new requirements which are shown below [6, 7]:

1. Applying the electric boundary condition to the nodes of the lead conductor region, in this work the operation voltage of OIP condenser bushing is 72.5kV and the test voltage for a dry power frequency withstand test according to IEC 60067-3 standard is $140\text{kV}_{\text{rms}}$. In ANSYS software that is done by loading the nodes of lead conductor with the maximum value of test voltage at 50HZ which equals to $(140\times\sqrt{2}\times10^{3}=197990V)$.
2. Applying grounded potential (0V) on the nodes of mounting flange and last layer of aluminum foils.

In harmonic analysis, all quantities are assumed to be changing with the frequency, and the solution of harmonic problems requires frequency-step calculation, which is used for the numerical solution in FE model, the solution is to calculate the distribution of electric potential and the maximum value of electric field in all region of this bushing.

2.2.2.*Solution Procedures*

The actual case model has be validated, and observed the distribution of electric potential and electric field inside and outside surface of bushing before doing any modification on this model. In this study, the modification cases will be done by changing the number of aluminum foils and OIP layers, increasing the length of aluminum foils layers, and changing the thickness of the OIP layer without any changes in the dimension of bushing and thickness of aluminum foils, to notice the effects of all modification cases on the distribution of electric potential and the electric field of the bushing, and compare the results of the modification cases with the results of actual case The modification cases were divided to as shown in Table.3

Table 3. modification cases of 72.5kV OIP bushing.

Modification cases	Describe of case	Number of case	Number of foil and OIP layers
First modification	Changing the number of the layers of aluminum foils and OIP	Case 1	14 foils 15 OIP
		Case 2	18 foils 19 OIP
Second modification	Changing the length of aluminum foils layers	Case 3	14 foils 15 OIP
		Case 4	16 foils 17 OIP
		Case 5	18 foils 19 OIP
Third modification	Changing the thickness of OIP layers	Case 6	14 foils 15 OIP
		Case 7	16 foils 17 OIP
		Case 8	18 foils 19 OIP
Fourth modification	Changing the thickness of OIP layers, and the length of aluminum foil layers	Case 9	14 foils 15 OIP
		Case 10	16 foils 17 OIP
		Case 11	18 foils 19 OIP

3. Simulation and Results

3.1. Actual Case

In this section, the simulation results are presented for electric potential and electric field distribution in all regions of 72.5kV OIP condenser bushing. The condenser body of this bushing contans16 layers of aluminum foils and 17 layers of insulation paper impregnated with mineral oil (OIP) .

To show the distribution of electric potential and electric field for this bushing a three regions will be taken from bushing model for all

modifications under this study as shown in fig.4. In addition of that each region will have one path, the details of each path are:

- path A: it is located in air side ,which start from the points of porcelain contacts with oil conservator , and end at the points which contacts the porcelain with flange.
- Path B: it is located inside the bushing, this path start from the lead conductor and end with the inner surface of the flange.
- Path C: it is located at the lower part of bushing and inside the transformer oil tank, which starts from the points contact the porcelain with the ring stress shield and ends from the points of (BCT extension) that contact with porcelain.

The distribution of electric potential and electric field in entire model of bushing show in figures.5 and 6 respectively.

From fig.5 it can be seen that , the voltage on lead conductor is 197990V (it connects to HV terminal) and decreasing gradually to (0V) at the flange.The electric field intensity is low when the electric potential difference is low, because the electric field intensity is obtained by divergence of electric potential (E=-∇v), for electric field the intensity of electric field concentrated at the sharp edges of the bushing, because the electric charge density on the sharp edges is higher than the flat surfaces according to equation(2) $\left(\nabla . E = \frac{\rho}{\varepsilon} \right)$.

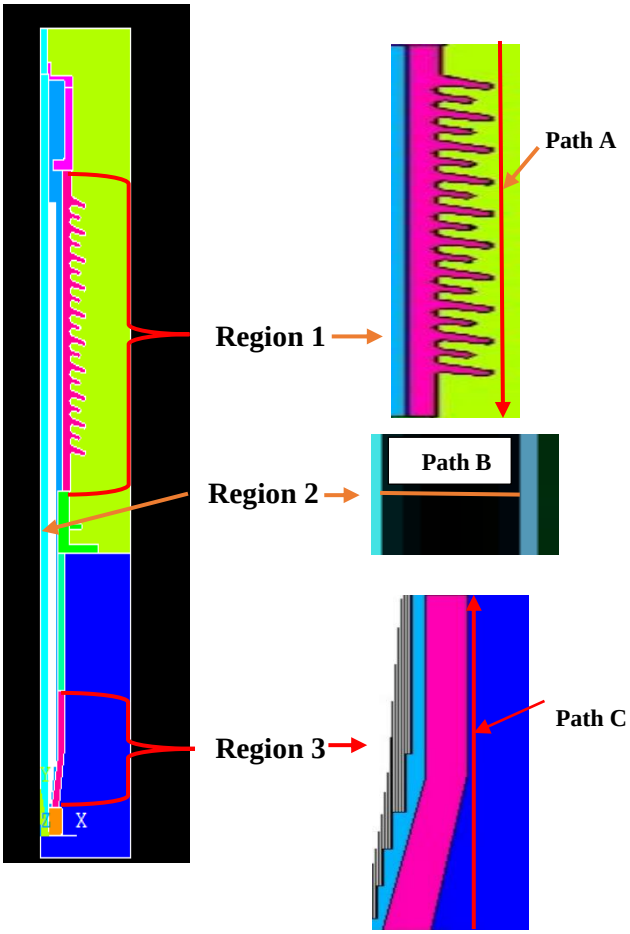

Figure 4. selected regions and Paths on the model of bushing

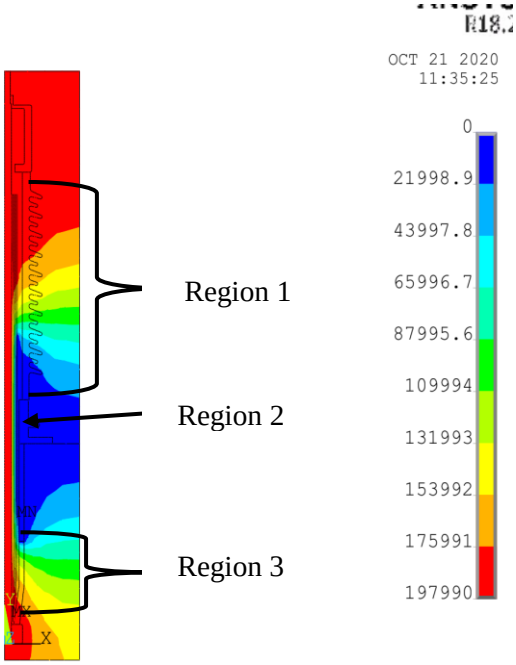

Figure 5. contour plot of electric potential distribution

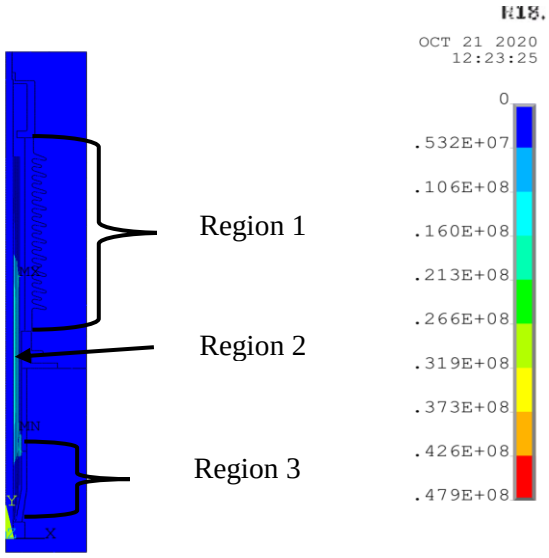

Figure 6. contour plot of electric field distribution

The maximum value of electric field in entire model of bushing occurs at the place, which have highest potential gradient. That place is the external surface of upper edge of last layer of aluminum foils (layer number 16), since the electric potential at external surface of upper edge's is high.

The distribution of electric potential and electric field in region(1) show in fig.7, it can be seen from path A the maximum value of voltage is (197990V) at the points of porcelain which contacts the oil conservator and decreasing gradually to (0V) at the points of porcelain which contacts the flange as shown in fig.7 (a).

From fig.7(b), it can be noted the maximum value of electric field intensity that concentrated on the external surface of porcelain surrounded by air side is (Ea=0.898kVrms/mm), While the maximum value of electric field intensity between two sheds is (Ec = 0.2863kVrms/mm). At the internal surface of porcelain which surrounding by mineral oil the maximum value of electric field intensity is (Eb= 0.7566kVrms/mm).

The graphs plotted in figures.8 and 9 represent the maximum and minimum values of distribution the electric potential and electric field along path A, it can be noted the different in voltage value along the external surface of porcelain due to the shape of porcelain sheds which have a lot of bends, and difference in insulation material. The external surface of porcelain surrounded by air while the internal surface of porcelain surrounded by mineral oil, this in turn will make the value of electric field is different between the porcelain and air. The difference in permittivity value between the porcelain and air will affect on the distribution of electric field between them, because the electric field depends on the value of permittivity for each materials, as it is inversely proportional to the permittivity value of the material.

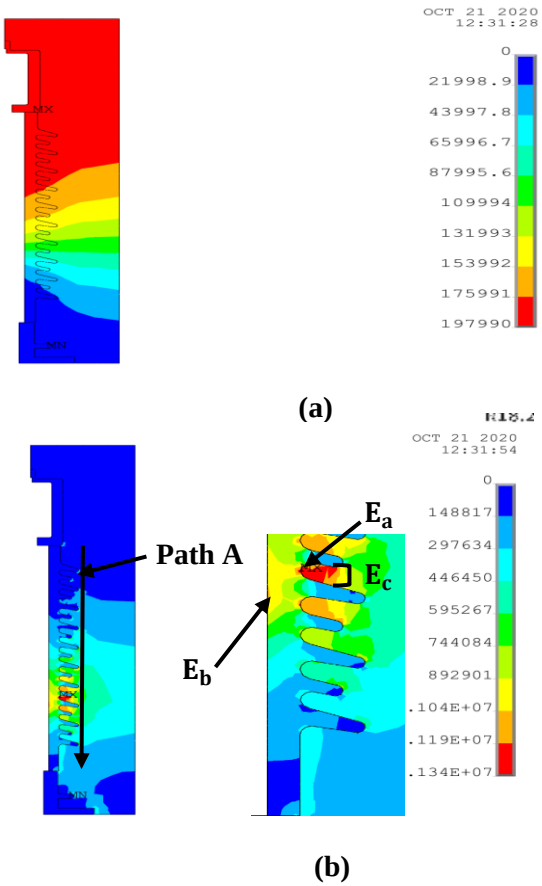

Figure 7. contour plots along path A of distribution (a) electric potential; (b) electric field

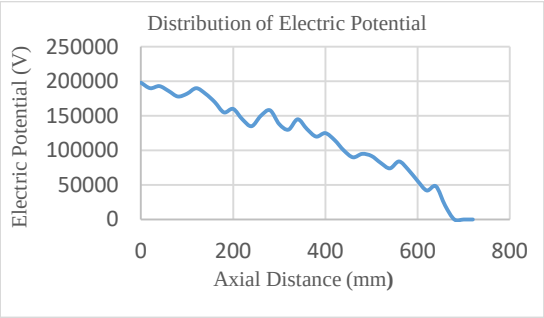

Figure 8. Distribution of electric potential

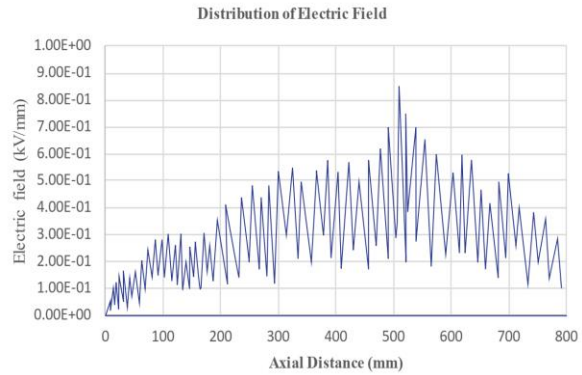

Figure 9. Distribution of electric field.

For path B, the distribution of electric potential and electric field show in fig.10, it can be noted the distribution of electric potential is linearly at each aluminum foil layer, the voltage at first layer of aluminum foil is (197536V) and gradually decreasing to (0V) at last layer of aluminum foil. The distribution of electric field shown in fig.10 (b) also is uniformly, and the radial electric field inside each layer of aluminum foils is zero, because aluminum foils are conductor material. The aluminum foils are used inside the bushing between the OIP layers to make the distribution of radial electric field is regular, and not concentrated of electric field stress at one point than other in insulation.

The graphs plotted in fig.11 shows the maximum and minimum value of electric potential along path B, and the average value of electric field intensity of the insulating paper, which is equal 5.4kVrms/mm. This value is less than the allowable value of breakdown electric field strength of Kraft paper (impregnated with transformer oil).

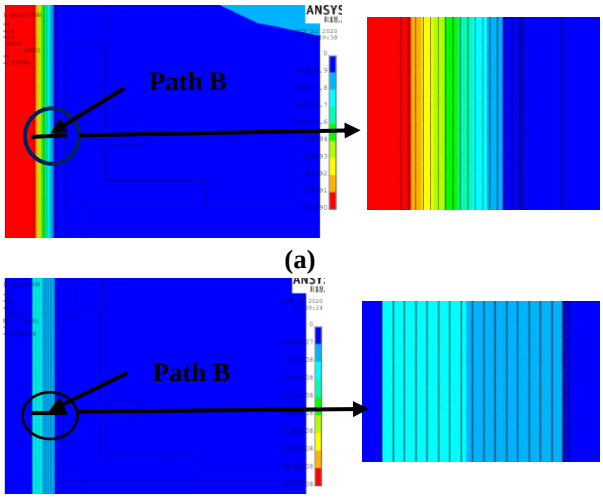

Figure 10. Contour plots along path B of distribution (a) electric potential; (b) electric field

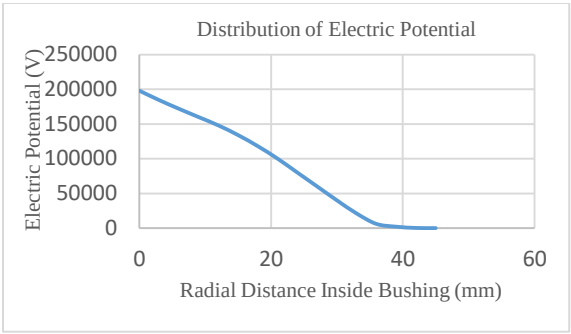

(a)

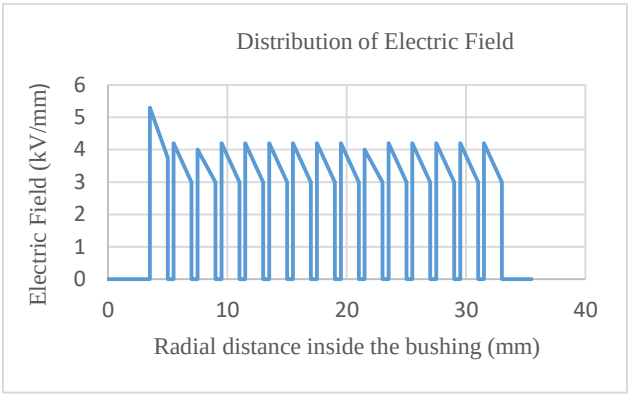

(b)

Figure 11. (a) distribution of electric potential (b) distribution of electric field

The distribution of electric potential and electric field along path C is shown in fig.12. On the lower part of porcelain at points which contacts the stress shield the voltage is equal to (197990V) and decreasing gradually to (0V) at (BCT extension) which is connected to the lower part of the flange.

The maximum value of electric field intensity that concentrated on the external surface of porcelain is E_r, which equal 2.47kVrms/mm is, while on the internal surface of porcelain is E_s equal to 5.105kVrms/mm.

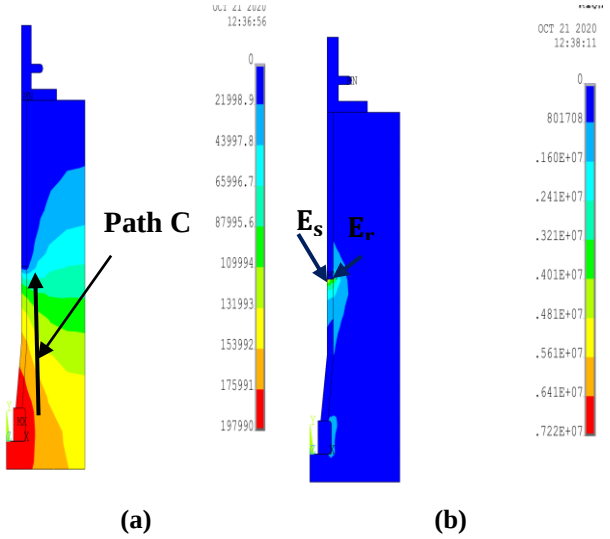

Figure 12. Contour plot along path C of distribution: (a) electric potential, (b)electric field

The maximum and minimum values of distribution of the electric potential and electric field along path C show in figures.13 and 14. At this path the porcelain is surrounded by mineral oil from the both side (same type of insulation material from both side), that lead to no different in voltage value along the external surface of porcelain compare with the porcelain in air side, also the porcelain in this part of bushing doesn't have sheds, that will make the electric field distribution along the external surface of porcelain is linearly.

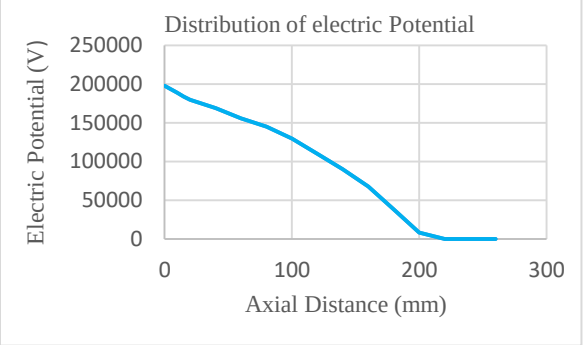

Figure 13. Distribution of electric potential

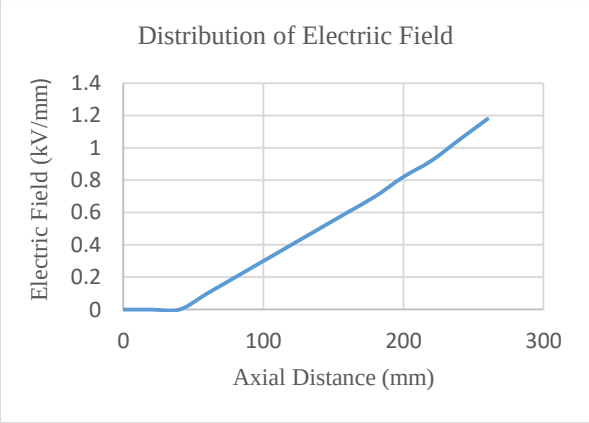

Figure 14. Distribution of electric field

3.2. First modification

In this section, it will be shown the simulation results for the distribution electric potential and electric field inside and outside surface of bushing in case1and case2 as the same in the actual case.

The maximum and minimum value of electric potential distribution along path A show in fig.15, it can be noted, the different in voltage value along the external surface of porcelain as same in the actual case.

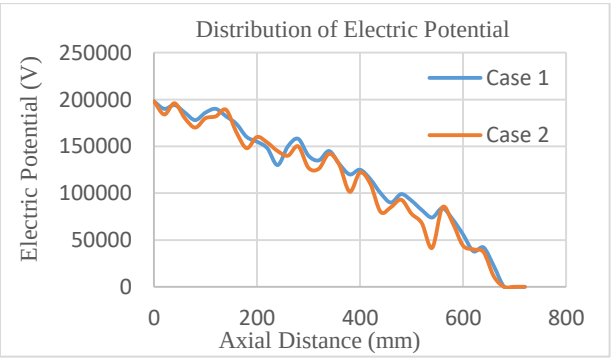

Figure 15. distribution of electric potential

The maximum value of concentrated electric field intensity on the external surface of porcelain is E_a, which is equal to $0.912kV_{rms}/mm$ in case1, and in case 2 is 0.848kv_rms/mm.While the maximum value of concentrated electric field intensity on the internal surface of porcelain is E_b, which is equal to $0.763kV_{rms}/mm$ in case 1, and in case 2 is $0.7212kV_{rms}/mm$. The location of maximum value of electric field intensity in case 1 and case 2 show in fig.16.

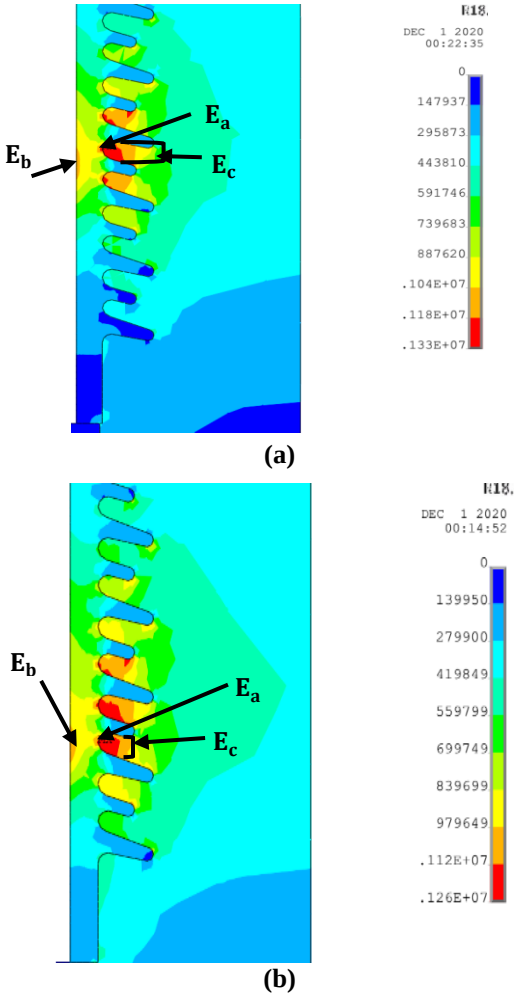

Figure 16. contour plot of electric field distribution (a) case 1 (b) case 2

When increasing the layer number of aluminum foils the gradation of voltage in aluminum foils become more regular along path B as shown in Table.4.

The graphs plotted of distribution the electric field along path A (in case 1 and case 2) show in fig. 17, it can be seen that the different in the distribution of electric field along the external surface of porcelain is the same in the actual case, for the same reasons that have been explained in the actual case, but the maximum values of electric field intensity on the external and internal surface of bushing different of each cases, depending on the number layers of aluminum foil and OIP, length and location of the aluminum foils for each cases.

Table 4. Voltage distribution of each aluminum foils along path B

foil number	Voltage distribution of aluminum foils (kVrms)		
	Actual case (16 foils)	Case 1 (14 foils)	Case 2 (18 foils)
1	127.27	126.4	128.8
2	116.6	114.5	119
3	106	102.3	108.8
4	96.3	91.5	100
5	85.55	80.3	90.7
6	77.2	70.42	82.5
7	67.8	60	73.53
8	59.53	50.98	66.4
9	50.8	41.29	58.4
10	43.13	32.8	51.4
11	35	23.82	43.98
12	27.8	15.83	37.3
13	20.22	6.7	30.4
14	13.51	0	24.18
15	7.2	-	17.6
16	0	-	11.7
17	-	-	4.8
18	-	-	0

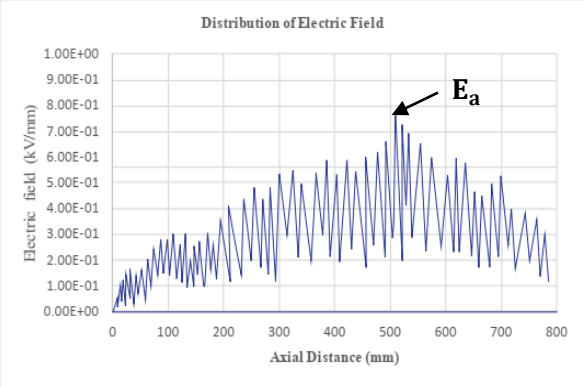

(a)

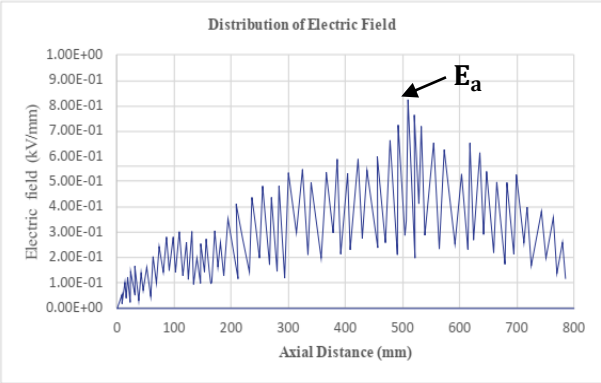

(b)

Figure 17. Distribution of electric field (a) case1 (b) case 2

For path B (in case 1 and case 2) the distribution of electric potential is linearly and gradient from the lead conductor to internal surface of the flange. In case 1 the voltage at the first layer of aluminum foils is (197471V) , while in case 2 is (197610V) and decreasing gradually to (0V) at the last layer of aluminum foils as shown in fig.18.

For path B (in case 1 and case 2) the distribution of electric potential is linearly and gradient from the lead conductor to internal surface of flange. In case 1 the voltage at the first layer of aluminum foils is (197471V) , while in case 2 is (197610V) and decreasing gradually to (0V) at last layer of aluminum foils as shown in fig.18.

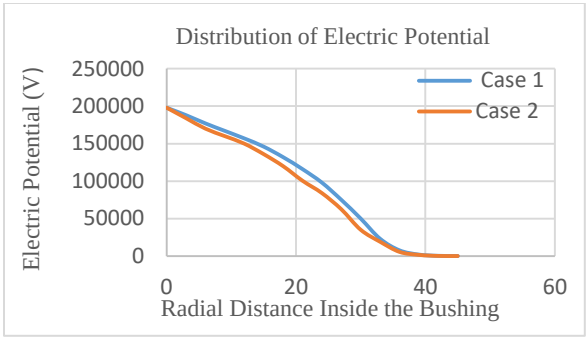

Figure 18. distribution of electric potential along path B

The distribution of electric field along path B shown in figures.19 and 20 respectively, The average value of electric field intensity of the insulating paper in case 1 is 6.5kVrms/mm, and in case 2 is 4.8kVrms/mm. the average value of electric field intensity in case 1 is more than allowable value of breakdown electric field strength of Kraft paper (impregnated with transformer oil).

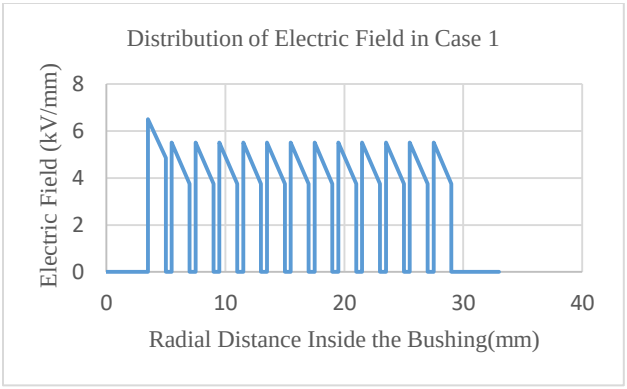

Figure 19. Distribution of electric field along path B in case 1

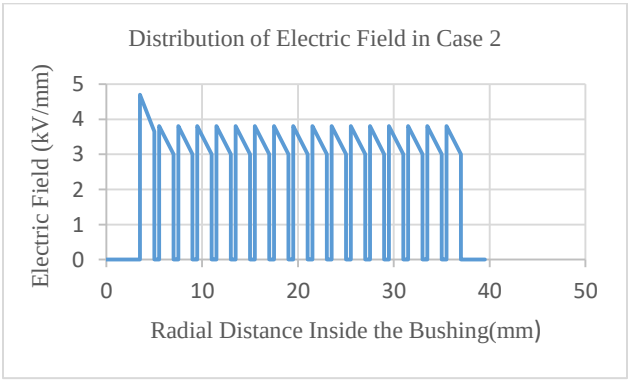

Figure 20. Distribution of electric field along path B in case 2

Fig.21 shows the distribution of electric potential along path C. The voltage at points which the porcelain contacts the stress shield is 197990V and decreasing gradually to (0V) at points which porcelain contacts the BCT extension (BCT is connected with the lower part of flange).

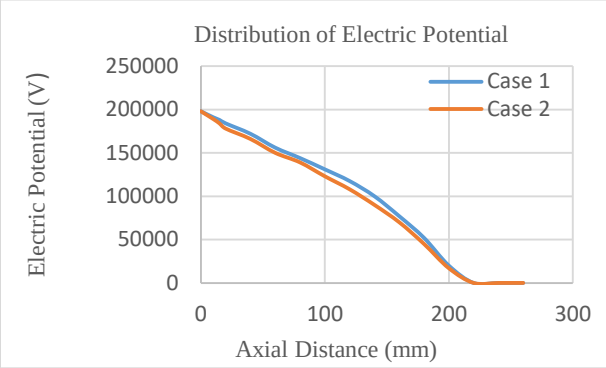

Figure 21. distribution of electric potential along path C in (case 1 and case 2)

For path C, the maximum value of concentrated electric field intensity on the external surface of porcelain in case 1 is ($E_r = 2.83kV_{rms}/mm$), and in case 2 is ($2.58kV_{rms}/mm$). While on the internal surface of porcelain in case 1 is (E_s= $4.101kV_{rms}/mm$), and in case 2 is ($3.2kV_{rms}/mm$).Fig .22 shows the location of maximum value of electric field intensity in case 1 and case 2.

The maximum and minimum value of the distribution of electric field along path C in (case 1 and case 2) show in fig.23.

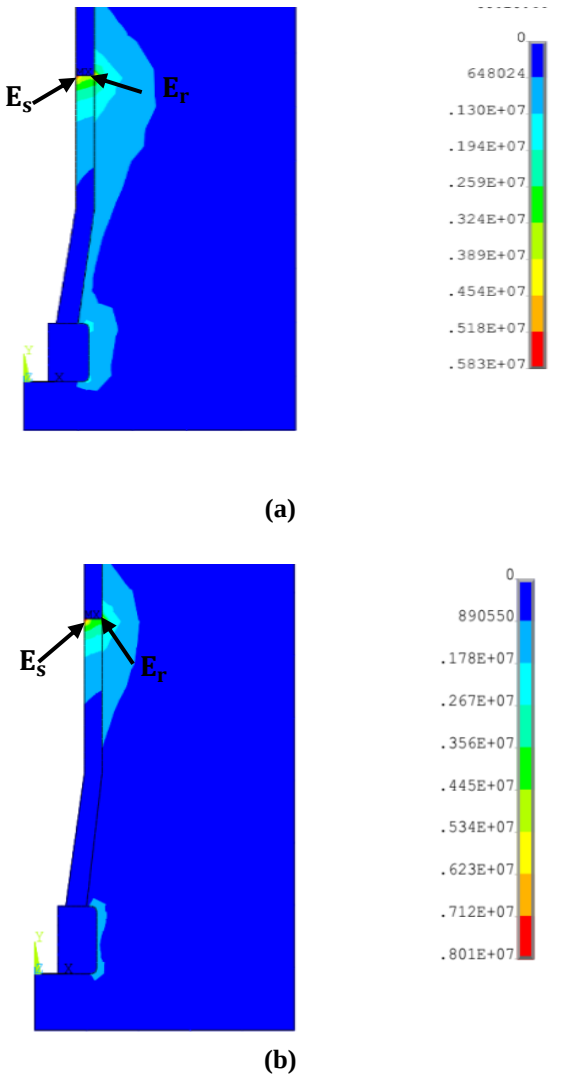

Figure 22. Contour plot of electric field distribution along path C (a) case 1 (b) case 2

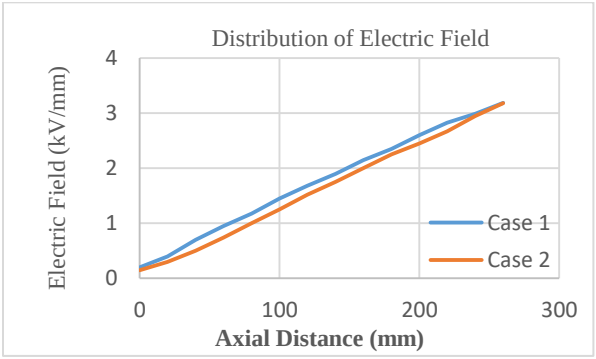

Figure 23. Distribution of electric field along path C in case 1and case 2

The maximum value of electric field intensity in the FE model of bushing in actual case and first modification are show in Table.5, and the average value of electric field along path B in actual case and first modification show in Table.6

Table 5. maximum value of electric field intensity in actual case and first modification

	Maximum value of electric field intensity (kV_{rms}/mm)		
	Actual case 16 foils	Case 1 14 foils	Case 2 18 foils
On the internal surface of porcelain along path A (E_b)	0.756	0.763	0.7212
On the external surface of porcelain along path A (E_a)	0.898	0.912	0.848
on the internal surface of porcelain along path C (E_s)	5.105	4101	3.2
on the external surface of porcelain along path C (E_r)	2.47	2.83	2.58

Table 6. average value of electric field in actual case and first modification

Average value of electric field along path B(kV_{rms}/mm)		
Actual case (16 foils)	Case 1 (14 foils)	Case 2 (18 foils)
5.4	6.5	4.8

From the results in table. 5, it can be noted that:

- When increasing the layers number of aluminum foils and OIP, the radial electric stress on the insulating papers was decreased (as shown in case 2, since the radial electric stress located on x-axis.
- Case 2, it is considered the best case compare with the actual case and case 1, because the electric field distribution inside and outside the surface of porcelain in the air side of the bushing is improved.

3.3. Second Modification

In this section, it will show the effect of increasing the length of aluminum foils layers on distribution of electric potential and electric field, with keeping the thickness of aluminum foils and OIP layers without any change.

The length of each layer of aluminum foils in all cases are show in Tables,7, 8 and 9 respectively.

Table 7. length of aluminum foils layers in actual case and case 4

Foil number	Length (mm) Actual case (16 foils)	Case4 (16 foils)	Foil number	Length (mm) Actual case (16foils)	Case 4 (16 foils)
1	1180	1205	9	835	860
2	1139	1164	10	794	819
3	1090	1115	11	752	777
4	1053	1078	12	713	738
5	1007	1032	13	683	708
6	964	989	14	635	660
7	918	943	15	600	625
8	876	901	16	560	585

Table 8. length of aluminum foils layer in case 1 and case 3

Foil number	Length (mm) Case 1 (14 foils)	Case3 (14foils)	Foil number	Length (mm) Case 1 (14foils)	Case 3 (14foils)
1	1180	1205	8	876	901
2	1139	1164	9	835	860
3	1090	1115	10	794	819
4	1053	1078	11	752	777
5	1007	1032	12	713	738
6	964	989	13	683	708
7	918	943	14	635	660

Table 9. length of aluminum foils layer in case 2 and case 5

Foil number	Length (mm) Case 2 (18foils)	Case 5 (18 foils)	Foil number	Length (mm) Case 2 (18foils)	Case 5 (18foils)
1	1180	1205	10	794	819
2	1139	1164	11	752	777
3	1090	1115	12	713	738
4	1053	1078	13	683	708
5	1007	1032	14	635	660
6	964	989	15	600	625
7	918	943	16	560	585
8	876	901	17	515	540
9	835	860	18	470	495

The distribution of electric potential in all these cases is linearly and uniform as shown in actual case and first modification. The voltage distribution along path B of each aluminum foils layer is show in Table.10, and the maximum value of electric field intensity for three paths of the bushing model show in Table.11.

Table 10. Voltage distribution of each aluminum foils in second modification

foil number	Voltage distribution of aluminum foils (kVrms)		
	Case 3 (14 foils)	Case 4 (16 foils)	Case 5 (18 foils)
1	126.4	127.27	128.8
2	114	116.6	119
3	102.3	105	108.8
4	91.9	96.3	100
5	79.9	84	90.7
6	70.4	77.2	82.5
7	60	67.8	73.53
8	50.98	59.53	66.3
9	41.29	50.8	58.4
10	32.8	43.13	51.3
11	23.82	35	43.98
12	15.83	27.8	37.3
13	6.7	20.22	30.26
14	0	13	24.11
15	-	73	17.6
16	-	0	11.73
17	-	-	4.8
18	-	-	0

The maximum value of electric field intensity for three paths of the bushing model show in Table.11.

Table 11. maximum value of electric field intensity in Second modification

	Maximum value of electric field intensity (kV_{rms}/mm)		
	Case 3 (14foils)	Case 4 (16 foils)	Case 5 (18 foils)
On the internal surface of porcelain along path A (E_b)	0.738	0.703	0.706
On the external surface of porcelain along path A (E_a)	0.714	0.880	0.822
on the internal surface of porcelain along path C (E_s)	3.520	4.462	4.270
on the external surface of porcelain along path C (E_r)	2.205	2.903	2.570

Table 12. Average value of electric field intensity in second modification

Average value of electric field along path B(kV_{rms}/mm)		
Case 3 (14 foils)	Case 4 (16 foils)	Case 5 (18 foils)
6.5	5.4	4.8

From table.12, it can be noted, the average values of electric field intensity along path B are remained constant on their values in first modification, it can be concluded that the radial electric stress not affected by increasing the length of the aluminum foils layer. Due to the radial electric field is on x-axis, and the length of aluminum foils on the y-axis.

3.4. Third Modification

In this section, it will be increased the thickness of the insulation paper (OIP) only for all previous cases. The thickness of OIP layer will be become 1.4mm.

The voltage distribution of each aluminum foils are show in Table.13, and the maximum value of electric field intensity are show in Table.14. Increasing the thickness of insulation paper (OIP) lead to decreasing the radial electric stress inside the bushing.

Table 13. Voltage distribution of each aluminum foils in third modification

Foil Number	Voltage distribution of aluminum foils (kVrms)		
	Case 6 (14 foils)	Case 7 (16 foils)	Case 8 (18 foils)
1	127.2	128.6	129
2	114.55	115.9	118
3	103.23	106	108
4	91.9	95.4	98.28
5	81.31	86.26	89.8
6	70	75.6	80
7	61.6	67.3	72.6
8	51.6	57.9	63.9
9	43.27	50	56.8
10	34	41.7	48.7
11	22.6	33.2	41
12	12	25.4	33.5
13	5.6	17.6	26.3
14	0	9.8	19.4
15	-	4.8	14.14
16	-	0	8.5

17	-	-	4.2
18	-	-	0

Table 14. maximum value of electric field intensity in third modification

	Maximum value of electric field intensity (kV_{rms}/mm)		
	Case 6 14 foils	Case 7 16 foils	Case 8 18 foils
On the internal surface of porcelain along path A (E_b)	0.765	0.730	0.723
On the external surface of porcelain along path A (E_a)	0.9	0.921	0.962
on the internal surface of porcelain along path C (E_s)	4.090	4.64	4.290
on the external surface of porcelain along path C (E_r)	2.65	2.64	2.706

Table 15. average value of electric field intensity in third modification

	Maximum value of electric field intensity (kV_{rms}/mm)		
	Case 9 14 foils	Case 10 16 foils	Case 11 18 foils
On the internal surface of porcelain along path A (E_b)	0.762	0.741	0.703
On the external surface of porcelain along path A (E_a)	0.975	0.886	0.936
on the internal surface of porcelain along path C (E_s)	4.093	3.975	3.215
on the external surface of porcelain along path C (E_r)	2.707	2.681	2.28

Table 16. Voltage distribution of each aluminum foils in fourth modification

Average value of electric field along path B (kV_{rms}/mm)		
Case 6 (14 foils)	Case 7 (16 foils)	Case 8 (18 foils)
5.656	4.8	3.8

3.5. Fourth Modification

This modification combines the second and third modification together, the voltage distribution of each aluminum foils along path B show in Table.16

Table.17 maximum value of electric field intensity in fourth modification

foil number	Voltage distribution of aluminum foils (kVrms)		
	Case 9 (14 foils)	Case 10 (16 foils)	Case 11 (18 foils)
1	127.2	128.6	129
2	114.55	116	118
3	103.23	106	108
4	91.9	95.4	98.28
5	81.31	86.26	89.8
6	70.7	75.6	80
7	61.6	67.3	72.6
8	51.6	57.9	63.9
9	43.27	50	56.8
10	34	41.7	48.7
11	22.6	33.2	41
12	12	25.4	33.5
13	5.6	17.6	26.3
14	0	10.18	19.4
15	-	4.8	14.14
16	-	0	8.5
17	-	-	4.2
18	-	-	0

The maximum value of electric field intensity are show in Table.17, it can be noted the maximum value of electric field intensity in case 11 is the best among than other cases.

Table.18 average value of electric field intensity in fourth modification

Average value of electric field along path B (kV_{rms}/mm)		
Case 9 (14 foils)	Case 10 (16 foils)	Case 11 (18 foils)
5.656	4.8	3.8

From Table 18, it can be noted that the radial electric stress along path B remained constant as in third modification.

4. Conclusion

In this paper, the effect of changing the number of aluminum foil layers and OIP,

increasing the length of aluminum foil layers and increasing the thickness of the OIP layers have been studied on the distribution of electric potential and the electric field of the bushing, with keeping the thickness of the aluminum foil layers unchanged. The conclusions can be summarized as follows:

1. Modeling of OIP capacitor bushing in 2D using FEM for classification of 72.5 kV.
2. The exact values of the electric voltage, the values of the electric field strength, and the nature of its distribution were obtained. Also, the locations of the maximum values of the electric potential and electric field on each portion of the OIP capacitor bushing were determined by applying the voltage at withstanding the power frequency test on the FE bushing.
3. The number of aluminum foil and OIP layers has an effect on the value of the radial electric field inside the porcelain, as increasing the aluminum foil and OIP layers to the appropriate number of layers lead to a gradual decrease in the value of the radial electric field from the edges of the central conductor to the edge of the flange, thus reducing the radial electric stress on insulation paper (OIP).
4. The increase in the thickness of the insulation layers has an effect on the decrease in the value of the radial electric field on the insulation paper (OIP), but at the same time it leads to an increase in the value of the electric field along the surface of bushing compared to the actual case, but remains less than the permissible values.
5. The best improvement was obtained by increasing the length of the aluminum foil and the thickness of the OIP layers in modification (of a 72.5kV bushing), where low values of electric field strength were obtained inside the bushing and on the outer surface of the porcelain on the side of air.

Acknowledgements

This work is supported by Electrical Department/ Faculty of Engineering/ Mustansiriyah University**.**

Conflict of interest

The publication of this article does not cause any conflict of interest.

Abbreviations

E	Electric field strength
V	Electrical potential
∇	Gradient operator
ρ	Electric charge density
ε	Permittivity of dielectric material
ε_o	Air or space permittivity
ε_r	Relative permittivity of dielectric material.

5. References

1. Nekahi, A., Stewart, B. G., and McMeekin, S. G. (2015). *"Electric field distribution on the outer surface of lower porcelain of an OIP transformer bushing-accumulation of metal-contained colloid"*. IEEE 11th International Conference on the Properties and Applications of Dielectric Materials (ICPADM) .pp. 632-635.
2. Illias, H., Tunio, M. A., & Mokhlis, H. (2012). "*Distribution of electric field in capacitor and surge arrester bushings*". IEEE International Conference on Power and Energy (PECon). pp. 973-978.
3. Arisoy, A., and Kalenderli, Ö. "*Electric field analysis of HVAC testing unit using finite element method"*. CiteSeerX Scientific

Literature Digital Library and Search Engine, Id, 59971339.

4. Smith, D. J., McMeekin, S. G., Stewart, B. G., and Wallace, P. A. (2012). *"The modelling of electric field, capacitance and dissipation factor of a high voltage bushing over varying frequency"*. 47th International Universities Power Engineering Conference (UPEC), pp. 1-6. IEEE, September.
5. Filipović-Grčić, D., Filipović-Grčić, B., and Poljak, M. (2017)." *Electric field at sharp edge as a criterion for dimensioning condenser-type insulation Systems*". Electric Power Systems Research, Vol. 152, pp. 485-492.
6. AvilaPriya, F., Kalaiselvam, K., Poongothai, K., Arun, R., & Prabakaran, T. (2015). "*Electric field calculation and material optimization of 765kV bushing using FEA*". International Conference on Computation of Power, Energy, Information and Communication (ICCPEIC), pp. 0064-0070. IEEE, April.
7. Ahmed, Zeeshan. (2011). "*Analysis of Partial Discharge in OIP Bushing Models."*
8. Feilat, E. A., Metwally, I. A., Al-Matri, S., and Al-Abri, A. S. (2013). "*Analysis of the root causes of transformer bushing failures".* International Journal of Computer, Electrical, Automation, Control and Information Engineering, Vol.7, No.6, pp. 791-796.
9. Chakravorti, S. (2017). *Electric field analysis*. CRC Press.
10. Ryan, H. M. (Ed.). (2001). "*High voltage engineering and testing ",* No. 32. Iet
11. Murty, K. K. (2017). "*Fundamentals of condenser bushings".* Transformers Magazine, Vol 4, No 5, pp. 30-37.
12. Mahmoudi, A., Moosavian, S. M., Kahourzade, S., and Ghiri, S. N. H. (2012). *"Capacitor bushing optimization via electrostatic finite element analysis".* International Journal if the Physical Sciences, Vol. 7, No. 2, pp.306 – 316.
13. Okabe, S., Hayakawa, N., Murase, H., Hama, H., & Okubo, H. (2006). *"Common insulating properties in insulating materials"*. IEEE transactions on dielectrics and electrical insulation, Vol.13, No.2, pp. 327-335.